Global Land Surface Backscatter at Ku-Band Using Merged Jason1, Envisat, and Jason2 Data Sets

Le Yang, Qinhuo Liu, *Member, IEEE*, Jing Zhao, and Lifeng Bao

***Abstract*—A unique method for investigating continental surfaces uses backscatter data measured by a radar altimeter at the nadir point of a satellite, in contrast to other microwave sensors designed to work at oblique angles, such as scatterometers and synthetic aperture radar. To improve the altimetry resolution over land, we generated $0.5^\circ \times 0.5^\circ$ merged altimetry backscatter maps covering 66° N to 66° S over the global land surface every six days for the period from January 2002 to June 2009 by combining three altimeter data sets (Jason1, Envisat, Jason2) in the Ku-band. The four backscatter products of Envisat RA2 from different retracking algorithms were evaluated prior to merging with the Jason1 and Jason2 data. The global pattern and the seasonal variation of the merged altimetry backscatter were examined, which show the merged results have better spatial sampling for the regional to global geophysical process due to the combination of three altimeters. To understand how the altimetry backscatter is related to land surface parameters, the advanced integral equation model for bare soil and water cloud model for vegetation are used to simulate the Ku-band backscatter response to soil and vegetation parameters at an incidence of 0°. Furthermore, we compared the time series of merged altimetry backscatter with the leaf area index (LAI) determined by an optical sensor and the backscatter coefficients obtained from a scatterometer (QuikSCAT) over seven selected vegetated areas over six years. The results confirm the sensitivity of ocean altimetry to vegetation. Further studies relating altimetry backscatter to geophysical parameter are needed.**

***Index Terms*—Backscatter, continental surfaces, leaf area index (LAI), radar altimeter.**

I. Introduction

MONITORING land surface characteristics at global or regional scales from space can contribute significantly in improving our understanding of land surface processes and their interactions with the atmosphere and biogeochemical cycle. The monitoring of vegetation, soil parameters, snow, and inland water has been conducted for many years through the use of various spaceborne sensors operating in different parts of the electromagnetic spectrum, such as the visible or infrared domains (AVHRR, MODIS) or the microwave domain, including passive microwave radiometers (SMMR, SSM/I) and active microwave sensors [scatterometer, radar altimeter, and synthetic aperture radar (SAR)].

Radar altimetry [1] was initially designed to measure the instantaneous sea surface height, wave height, and backscatter of the ocean surface by transmitting radar pulses and receiving the backscatter energy at the nadir point of a satellite. Altimetry data are also extremely useful for a broad range of ice and land applications, including topography mapping for Antarctica and Greenland [2], continental water-level monitoring [3], [4], and digital elevation model (DEM) construction for land surfaces [5], [6]. In addition to height measurements, the normalized radar backscatter coefficient (σ^0) over the land surface is also provided. The σ^0 value measured by radar altimetry is unique for investigating continental surfaces, rather than that measured by a scatterometer[7] or SAR [8] for radar altimetry observes strictly in the vertical dimension.

Ridley *et al.* [11] showed that Topex/Poseidon backscatter measurements over the Simpson Desert in Australia are strongly affected by variations in soil moisture and by the presence of dew. Bramer *et al.* [12], [13] presented an analysis of Envisat RA2 global backscatter performance on both the Ku- and S-band, particularly over dry land surfaces, and found that σ^0 is very stable over the identified land calibration zones. Papa *et al.* [14] presented the first global-scale results regarding the geographical dynamics of backscatter over land surfaces using Topex/Poseidon dual-frequency backscatter data from 1992 to 2001. All of these studies have demonstrated the potential of backscatter data measured by radar altimetry for land surface studies on a regional or global scale. However, those studies have only used the single altimeter data and evaluated the backscatter in a qualitative way by analysis the spatial and temporal distributions.

To date, the altimetric series of Topex/Poseidon, Jason1, Jason2, ERS1, ERS2, and Envisat provide 20 years of continuous and homogeneous observations, which enable long-term analyses related to global climate change. However, the spatial and temporal coverage of single radar altimetry is low because the swath width of an altimeter is only approximately 10 km at the nadir point of the satellite. The repeat cycle of Jason1 is ten days, and the ground track space at the equator is 315 km. The repeat cycle and ground track space at the equator for Envisat RA2 are 35 days and 77 km, respectively.

The aim of this study is to merge multiradar altimetry backscatter measurements over land surfaces to increase the spatial and temporal resolution. Microwave scattering models

Manuscript received May 13, 2013; revised December 7, 2013 and March 25, 2014; accepted May 22, 2014. This work was supported in part by the Chinese Academy of Sciences Special Fund under Grant KZZD-EW-TZ-18, by the National Basic Research Program of China (973 Program) under Grant 2013CB733401, and by the Chinese Natural Science Foundation 41001212, and by the State Laboratory of Remote Sensing Science Young Scientists Foundation under Grant 10QN-05.

L. Yang, Q. Liu, and J. Zhao are with the State Key Laboratory of Remote Sensing Science, Institute of Remote Sensing and Digital Earth, Chinese Academy of Science, Beijing 100101, China (e-mail: yangle@radi.ac.cn; qhliu@irsa.ac.cn; Zhaojing1@radi.ac.cn).

L. Bao is with theState Key Laboratory of Geodesy and Earth's Dynamics, Institute of Geodesy and Geophysics, Chinese Academy of Sciences, Wuhan 430077, China (email: baolifeng@whigg.ac.cn).

Color versions of one or more of the figures in this paper are available online at http://ieeexplore.ieee.org.

Digital Object Identifier 10.1109/TGRS.2014.2328616

for soil and vegetation are used separately to simulate the backscatter response to soil and vegetation parameters for different frequencies and incidence angles, particularly within the Ku-band at 0°. The merged altimeter backscatter is derived by cross-calibrating the backscatter histogram of three altimeter measurements to eliminate the systematic differences. The global pattern and time series of merged altimetry backscatter data over desert and forest areas are presented.

The satellite data and the data merging method are presented in Section II. Section III describes the model simulation results and explores the possibility of retrieving geophysical parameters from multialtimeter data. Section IV presents results on a global scale and the geographical dynamics of backscatter over typical land cover areas. Section V gives conclusions and perspectives.

II. Datasets and Merging Methods

Backscatter data from three radar altimeters were used in this study: Jason1 [15], Jason2 [16], and Envisat Radar Altimeter (RA2) [17]. Unlike Jason1/2, Envisat RA2 provides five sets of backscatter coefficients from four retrackers (Ocean, Ice1, Ice2, SeaIce). To determine which backscatter coefficient data set from Envisat RA2 should be merged with the Jason1 and Jason2 measurements, the four sets of Envisat RA2 backscatter coefficient data were compared.

A. Datasets

The Jason1 and Jason2 satellites were launched on December 7, 2001 and June 20, 2008, respectively, by National Aeronautics and Space Administration and Centre National d'Etudes Spatiales to ensure continuity of the oceanographic observations provided by the remarkable mission Topex/Poseidon. Poseidon2 and Poseidon3 onboard the Jason1 and Jason2 have a 9.91-day repeat cycle and provide measurements in the Ku (13.6 GHz) and C (5.4 GHz) bands. Observations along the ground track of all ocean and continental surfaces from these altimeters are made from 66° N to 66° S. Jason1 assumed a new orbit halfway through its original ground track in mid-February 2009 and encountered an anomaly at the end of February 2012. Currently, Jason2 is located on the former orbit of Topex/Poseidon (before 2002) and Jason-1 (before February 2009). Envisat was launched on March 1, 2002 by ESA (European Space Agency). RA2, onboard the Envisat, has a 35-day repeat cycle and provides global along-track measurements in the Ku and S (3.5 GHz) bands up to the latitude limit of 81.5° N/S. The Envisat satellite moved to a new lower orbit on October 22, 2010 and stopped transmitting data in April 2012. The footprint size of all three altimeters is approximately 10 km, and the ground tracks have a maximum drift of 1 km.

In this paper, we only used backscatter data for the Ku-band (13.6 GHz, 2.1 cm), which is the main working frequency for both Jason1/2 and Envisat RA2. Backscattering coefficient measurements expressed in decibels (dB) were extracted from the geophysical data record (GDR) products of the three altimeters from January 2002 to June 2009 provided by Archiving, Validation and Interpretation of Satellite Oceanographic Data (AVISO). The backscatter measurement errors are less than 1, 0.7, and 0.4 dB for Jason1, Jason2, and Envisat RA2, respectively. The backscatter recorded in the GDR is already corrected for atmospheric attenuation, and unbiased σ^0 values were recorded by the ocean surface topography mission (OSTM)/Jason2 data products related to Jason1.

The data points for which the square of the off-nadir angle of the altimeter was less than 0.2° were selected for analysis, according to the data editing criteria of Jason1. To avoid the inclusion of water and ice measurements in the land surface data, we masked the data over the ocean, rivers, lakes, and ice using a surface-type flag based on bathymetry information. Thus, the phase global land surface refers to continental surfaces between 66° N and 66° S without ocean, rivers, lakes, or ice for the remainder of this article. The land surface type is based on the MODIS Land Cover Classification product (MOD12C1) of the International Geosphere-Biosphere Programme standard [18] with a resolution of 0.05°.

B. Envisat RA2 Data Comparison

Five sets of backscatter data are available in Envisat RA2 products from Ocean, Ice1, Ice2, and SeaIce retrackers. The ocean retracker is based on a modified Hayne model and is optimized for ocean surfaces. The Ice1 retracker is developed to provide optimal heights over continental ice sheets using an OCOG (Offset Center of Gravity) approach. The Ice2 retracker, which is designed for ice caps, detects the waveform edge and fits an error function to the leading edge and an exponential decrease to the trailing edge. An additional set of parameters is available for Ice2 by resampling part of the waveform called the "Ice2 Leading Edge." The fourth retracker is designed for the quasi-specular echoes returned from sea-ice, with thresholding on the waveform leading edge. For a detailed description of the four retrackers, see [17]. The four backscatter values in the Ku-band of the Envisat RA2 products, excluding the "Ice2 Leading Edge" backscatter values, are analyzed here.

One cycle of Envisat RA2 data (from May 26, 2008 to June 30, 2008) over the global land surface was extracted. The percentage of valid backscatter results ($0\ \text{dB} < \sigma^0 < 40\ \text{dB}$) for the Ocean, Ice1, Ice2, and SeaIce retrackers were 68.96%, 99.85%, 78.10%, and 99.85%, respectively. We calculated the backscatter differences between each pair of retrackers (see Fig. 1).

The statistics in Fig. 1 show large variability among the backscatter values estimated by the Ocean, Ice1, Ice2, and SeaIce retrackers. For the retracker combinations, the shape of the histogram is narrow and high peaked for Ice1-SeaIce and Ocean-Ice2, reflecting the similarity in those pairs, with median backscatter value differences of -1.57 dB for Ice1-SeaIce and 2.18 dB for Ocean-Ice2. This result arises because the Ocean and Ice2 retrackers both fit the return waveform to waveform models, whereas the Ice1 and SeaIce retrackers utilize threshold-based algorithms. Furthermore, the backscatter of the SeaIce retracker is systematically higher than those of the other three retrackers, followed by the backscatter of the Ice1, Ocean, and Ice2 retrackers. The median values for SeaIce-Ice1,

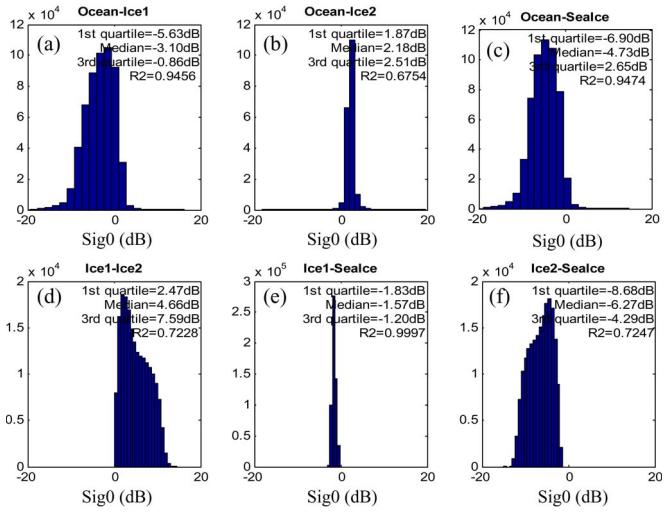

Fig. 1. Histograms of backscatter differences between the four Envisat RA2 retrackers (Ocean, Ice1, Ice2, and SeaIce) covering one cycle (May 26, 2008 to June 30, 2008) over the global land surfaces.

Ice1-Ocean, and Ocean-Ice2 were 1.75, 3.10, and 2.18 dB, respectively. The correlation coefficients between each pair of retrackers are also shown in Fig. 1. All of the correlation coefficients were high. The greatest correlation was observed between Ice1 and SeaIce $(R2 = 0.9997)$, and the smallest correlation occurred between Ocean and Ice2 $(R2 = 0.6754)$.

The analysis of the four RA2 retrackers Ku-band backscatter data over global land surface indicated that the four RA2 values varied greatly with the largest difference is -6.27 dB between Ice2 and SeaIce, the smallest difference is -1.57 dB between Ice1 and SeaIce. The backscatter values of the SeaIce and Ice1 retrackers were systematically larger than those of the Ocean and SeaIce, which were highly correlated with each other. Therefore, we chose to merge the backscatter data from the Ocean retracker of Envisat RA2 with the Jason1/2 backscatter measurements.

C. Backscatter Merging Method

Three steps were used to merge the multiradar altimetry data: data quality control, cross-calibration and extrapolation. The valid backscatter range over the ocean is 7 – 30 dB, according to Jason1 data-editing criteria. Because of the vegetation and soil attenuation, the volume scattering results in a lower backscatter coefficient than that of surface scattering over ocean [19]. We used the valid backscatter range over land of 0 – 30 dB for Jason1, Jason2, and Envisat RA2.

The cross-calibration of two altimeters requires independent and coincident σ^0 observations to correct for any systematic differences between σ^0 estimates from the two altimeters. However, a large and accurate calibration data set is not available. As an alternative, we employed an empirical technique to cross-calibrate σ^0 using only the σ^0 histograms from the different instruments [20]. Assuming that the backscatter distribution measured by altimetry is relatively stable over a sufficiently large geographical region and for sufficiently long time periods, the systematic differences between backscatter estimates from two altimeters can be identified based on comparisons of their

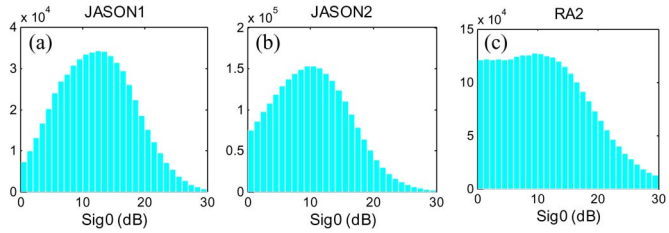

Fig. 2. Histograms of backscatter measurements (in decibels) for June 2008 to June 2009 over the global land surface from (a) Jason1, (b) Jason2, and (c) Envisat RA2.

backscatter histograms. The data were cross-calibrated using Jason2 backscatter measurements from June 2008 to June 2009 and Jason1 from January 2002 to June 2008 as a reference. Fig. 2 shows the backscatter histograms from Jason1, Jason2 and Envisat RA2 for June 2008 to June 2009 over a global land surface. The total number of observations used to generate the histogram for Jason2 is greater than that for Jason1 due to the improved tracking method used for Jason2 [17], and the number of RA2 observations is greater than that of both Jason1 and Jason2 due to its intense spatial coverage.

We computed a cumulative distribution function (CDF) for the two altimetry backscatter distributions and fit a smooth spine to the fixed CDF. The cumulative percentage point for each binned value (σ^0_a) of the CDF to be adjusted was then determined. From the spline fit to the fixed CDF, we determined the value σ^0_f corresponding to the cumulative percentage value. Each backscatter value was adjusted by an amount of $\sigma^0\_a - \sigma^0\_f$. The bin step is important to the cross-calibration process because random errors tend to be cancelled within a given bin only if the bins contain a sufficient number of observations. We took the bin step as 1 dB for cross-calibrating Jason1, Jason2, and RA2 from June 2008 to June 2009 and as 3 dB for Jason1 and RA2 from June 2006 to June 2008. Fig. 3 shows the CDF of the three altimeters before and after the cross-calibration step. It can be seen that this adjustment brought the three histograms into exact agreement. However, corrections obtained using this method are susceptible to errors at σ^0 values near the tails of the histograms, where there are a few observations and random errors in individual measurements that do not, in general, average to zero. Therefore, σ^0 was divided into 40 equally sized bins to ensure that corrections were computed only for the σ^0 bins containing a sufficient number of observations.

Finally, the cross-calibrated σ^0 values of the three altimeters were interpolated on a $0.5^\circ \times 0.5^\circ$ grid for six-day intervals; for this step, we used the inverse distance-weighted method [21]. The σ^0 value for each grid is determined by the following equations:

$$S_{(i,j)} = \frac{\sum_{(k=1)}^{n} S(k) * W_k}{\sum_{(k=1)}^{n} W_k} \tag{1}$$

$$W_k = \frac{1}{d_k^m} \tag{2}$$

where $S_(i,j)$ is the interpolated result for grid(i,j). k is the number of measurements $S(k)$within the grid(i,j). The weight

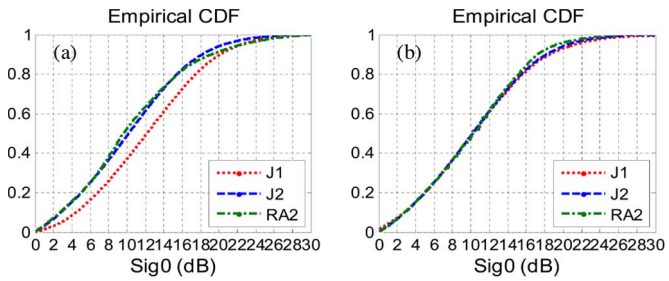

Fig. 3. The cumulative probability distribution function (CDF) of the backscatter measurements (dB) for the altimeters from Jason1 (green dotted line), Jason2 (blue dashed line) and Envisat RA2 (red dash-dot line) from June 2008 to June 2009 over global land surfaces before (a) and after (b) cross-calibration with Jason2 as a reference.

W_k is inversely proportional to the distance d_k from the σ^0 measurement to the center point of the grid. The exponent m is taken as 2. Data were smoothed and extrapolated using a Loess filter of $16^\circ \times 8^\circ$ (gaps due to missing data were filled, and the signal was strongly smoothed).

III. Theoretical Basis of the Altimetry Backscatter Over Land

Radar measurements are primarily a function of surface roughness, soil moisture, and the size, shape, moisture content, number density, and spatial distribution of all canopy constituents. The root-mean-square (RMS) height and correlation length are two important parameters describing the -geometric surface roughness of soil. The smaller the RMS height and the lower the correlation length, the smoother the surface. Great sensitivity differences in the surface backscatter signals to the surface properties exist at different frequencies and incidences. To analyze the backscatter coefficient measured by a nadir-viewing altimeter, we used the advanced integral equation model (AIEM) and water cloud models to simulate the backscatter at an incidence angle of 0° for bare soil and vegetation, respectively. Because there is no polarization difference at an incidence and observation angle of 0°, the following results are shown for the HH polarization.

A. Bare Soil Model

The AIEM model [22]–[24] can simulate surface emission and scattering signals for a wide range of rough surface parameters and for high-frequency observations. Shi *et al.* [25] evaluated the capability of AIEM to simulate high-frequency and high-incidence surface emission signals and compared their findings with a large set of field observation data. The results showed excellent agreement, with RMS heights of 2.6 and 3.9 cm obtained for selected roughness profile measurements conducted at each field site at frequencies between 5.05 and 36.5 GHz. In our simulation, the soil water content varies from 0.02 to 0.5 with a step of 0.02 (the unit is 1), the RMS height ranged from 0.25 to 3.5 cm with a step of 0.25 cm, and the correlation length ranged from 2.5 to 30 cm with a step of 2.5 cm. The Gaussian correlation function and Fresnel reflection coefficient as approximated by a transition were used.

Fig. 4 shows the results obtained for different incidence angles at a frequency of 13.6 GHz. For the two roughness parameters [see Fig. 4(a) and (b)], the backscatter at 0° declined steadily with increasing RMS height and decreasing correlation length, which differs from the results obtained at other angles. Furthermore, the backscatter at small incidence angles (below 20°) can better represent the wide range of roughness variation than oblique observations, particularly at lower RMS heights and larger correlation lengths. For the soil moisture [see Fig. 4(c)], the curves of the backscatter versus volume water content (VWC) are similar at different incidence angles, which indicate that the sensitivity of backscattering in the Ku-band to soil moisture is similar over a range of angles.

Other than the geometric roughness, the large-scale roughness (slope caused by elevation) is also an important factor to the altimetry backscatter measurements. When there is slope, the incidence of the altimeter is no longer 0°. However, slope has as similar effect on sigma0 as geometric roughness; the steeper the slope, the less power backscatters to the altimeter.

Therefore, we can conclude that the backscatter coefficient measured by an altimeter with a nadir-view configuration is much more sensitive to geometric surface roughness and large-scale roughness than a scatterometer or SAR, particularly for relatively smooth surfaces (lower roughness conditions). Furthermore, there are unique monotonically decreasing relations between the backscattering observed at 0° and the roughness.

B. Vegetation Model

A number of radar backscatter models have been developed for various types of vegetation. Several models have treated the canopy as a horizontally homogeneous medium, such as the water cloud model [26] and the Michigan microwave canopy scattering model (MIMICS) [27]. Discontinuous radar backscatter models [28], [29] were developed by considering the gap between the crown and the real structure of the trees, particularly for forests. Because the footprint size of an altimeter is as large as approximately 10 km, we chose the water cloud model, in which vegetation canopy is modeled as a lossy volume of scattering dielectric disk and cylinder elements, bounded by air above and by a scattering soil surface below without considering the coherence effect.

The model is achieved by adapting the MIMICS model by eliminating all the mechanisms related to the trunk layer. Therefore, the total backscatter consists of the incoherent summation of the four components as

$$\sigma^0_{pq} = \sigma^0_{pqv} + \sigma^0_{pqs} + \sigma^0_{pgvs} + \sigma^0_{pqsvs} \tag{3}$$

where the subscripts p and q denote the polarization of the incident and scattered wave, respectively. σ^0_{pqv} represents the direct scattering from the leaves and branches of the vegetation. σ^0_{pqs} represents scattering from soil surface attenuated by the vegetation. σ^0_{pgvs} represents the mutual coupling backscatter of vegetation and soil surface. σ^0_{pqsvs} represents the soil–vegetation–soil interaction return. A detailed discussion and calculation of those terms is given by [27].

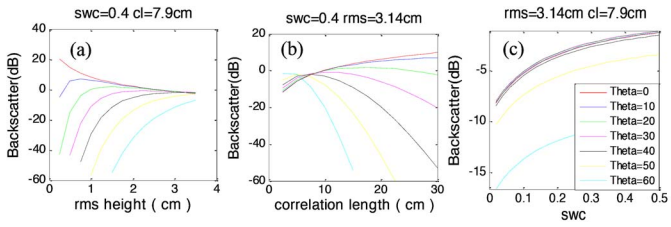

Fig. 4. Backscatter at the HH polarization versus (a) RMS height, (b) correlation length, and (c) VWC at a frequency of 13.6GHz for different incidence angles: 0° (red solid line), 10° (blue dotted line), 20° (green dashed line), 30° (magenta dashed line), 40° (black dotted line), 50° (yellow solid line) and 60° (cyan dashed line).

The density $(1000/\ \mathrm{m}^3)$, size (diameter $= 2$ cm, thickness $=$ 0.1 cm) and moisture (0.55) of the leaf and the density $(8/\ \mathrm{m}^3)$, size (length $= 75$ cm, diameter $= 0.7$ cm) and moisture (0.42) of the branch are fixed. We only increased the crown height from 0m to 30m. Due to the incidence angle and large footprint of radar altimeters, other factors, such as variations in leaf clumping or branch orientation, have a smaller impact on the altimetry backscatter.

Fig. 5(a) and (c) represent the backscatter observed by radar altimetry for the Ku-band at 0° and that measured by QuikSCAT of the Ku-band at 40°, respectively. The scattering mechanism is much simpler due to the weaker penetration capability of the Ku-band with its short wavelength (2.2 cm) compared with that of the L-band (21.4 cm) [see Fig. 5b, 5c]. In Fig. 5(b), the dominating scattering mechanism is the direct ground return. The contributions of crown–ground return, direct crown return, and ground–crown–ground return are not significant. For short wavelength of Ku-band [see Fig. 5a], the contributions of crown–ground return and ground–crown–ground return are too small to be displayed. However, the direct crown return replaced the direct ground return to be the main contributor when the crown height is larger than 20 m.

The total backscatter from QuikSCAT [see Fig. 5c] increases with increasing crown height, but only accounts for the direct crown return and is not sensitive to increasing crown height when the crown height is larger than approximately 5 m. In longer wavelengths of the L-band [see Fig. 5d], the response of the total backscatter to crown high is similar to that in Ku-band with bigger influences of crown–ground return and ground–crown–ground return.

The difference between the backscatter responses of Ku-band at incidence of 0° and 40° is from the backscatter at 0° responds to the scattering from soil and understory vegetation through forest gaps by penetrating deeper than that at 40°. The saturation value of the backscatter to the crown height is larger in the altimeter than that of the scatterometer, because the backscatter observed at the nadir view decreases with the growth of vegetation as long as the altimeter can "see" the ground through the tree gaps.

The threshold value for the switch between the dominating scattering mechanisms and the saturation point can differ for various vegetation types because the water cloud model used in this study simplifies the vegetation canopy, and the leaf density that normally decreases after a certain stage of canopy

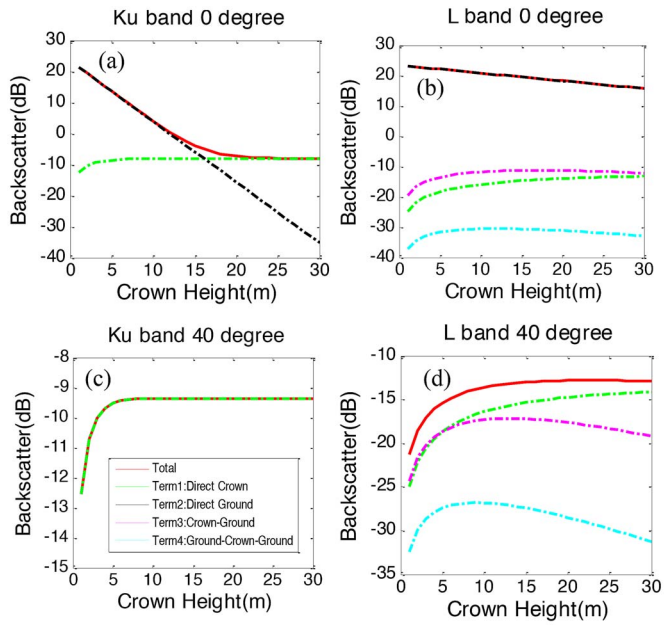

Fig. 5. Backscatter for HH polarization versus crown height (m) for the L-band at incidence angles of 0° (a) and 40° (b) and for the Ku-band at incidence angles of 0° (c) and 40° (d). The total backscatter (red solid line) consists of direct crown return (green dashed line), direct ground return (black dashed line), crown–ground return (magenta dashed line), and ground–crown–ground return (cyan dashed line).

growth. However, the overall trend and the dominated scattering mechanism are reliable.

Therefore, the backscatter measured by QuikSCAT directly responds to the scattering elements of the canopy, such as the leaves and branches, before the canopy is not too dense to be penetrated by the Ku-band measurements at high incidence angles. The radar altimetry measurements at the nadir point of a satellite decrease with increasing crown height. Backscatter measured by radar altimetry responds to ground scattering from soil and understory vegetation by penetrating deeper into the canopy and through forest gaps.

IV. Evaluation of the Merged Altimetry Backscatter

A. Global Pattern and Seasonal Variation Analysis

1) Mean Global Image Analysis: As the first step in evaluating the usefulness of the merged radar altimetry backscatter, we compared the global and regional patterns for different seasons. Figs. 6 and 7 show the mean monthly values (three cycles of Jason1 and Jason2, one cycle of Envisat RA2) for July, 2008 and January 2009. Fig. 6(a) shows the mean backscatter coefficient obtained by merging the Jason1, Envisat RA2, and Jason2 data for the Ku-band over the global land surface. Fig. 6(b)–(m) show the values for Jason1, Jason2, and Envisat RA2, respectively. The data are continuous in Fig. 6(a) and discontinuous in Fig. 6(b)–(m). Each point in Fig. 6(b)–(m), represents a backscatter measurement over a footprint of approximately 10 km (not in accordance with the axis scale). No data are available between ground tracks.

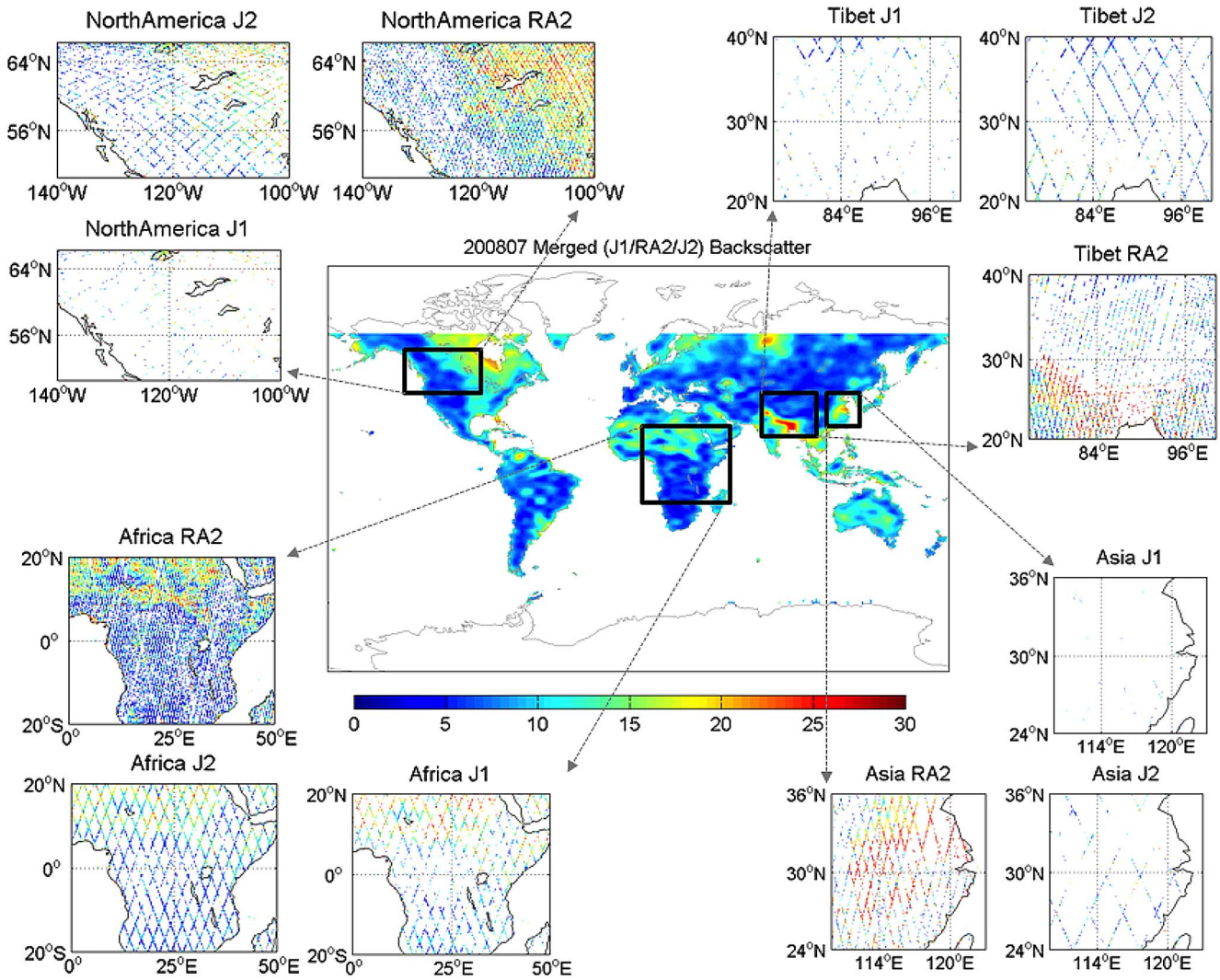

Fig. 6. Ku-band backscatter coefficient map (in decibels) of July 2008 of global merged data (a) and Tibet (b), (c), and (d); Asia (e), (f), and (g); Africa (h), (i), and (j); and North America (k), (l), and (m) for Jason1, Jason2, and Envisat RA2, respectively.

The track ability of Jason1 over land is the worst among the three altimeters. Data are seriously missing in eastern [see Fig. 6(e)] and northern China [see Fig. 6(b)] and on the west coast of North America [see Fig. 6(k)]. The tracking ability of Jason2 has improved over that of Jason1. The amount of data acquired by Envisat RA2 is superior in the way of the higher spatial resolution and denser ground tracks. The numbers of valid backscatter coefficient results over land (excluding rivers, lakes, and continental ice) for Jason1, Jason2, and RA2 were 52 457, 291 765, and 717 844 for January 2009, respectively. Furthermore, the global mean value of Jason1 was the largest (12.73 dB), and that of RA2 (5.46 dB) was the lowest.

It can be seen that the high backscatter values arise from flat surfaces such as large river basins (U.S. Great Lakes, the Yangtze River Delta in China, and the Ganges Plain in India), the Sahara Desert in Africa and the Australian plains. The backscatter measurements are low over the Himalayan, Andes, and Rocky Mountains, which is consistent with previous findings obtained from Topex/Poseidon altimetry data [14].

These patterns are examined in more detail by regions in the following.

Eurasian continent: The region around 30° N of eastern China is mainly cropland and mixed forest. For the merged results, the high value is located at the estuarine floodplain, and the low value is located at the hilly area at the southeast and northwest parts. This pattern is mainly captured by the RA2 backscatter, which is not evident at the Jason2 for its sparse ground tracks. The maximum of the merged value is 27.01 dB in July and 25.12 dB in January.

Tibetan plateau: The Tibetan plateau is the world's highest plateau (an average elevation exceeding 5000 m) and is bounded by the Himalayan mountain chains to its south, where the altitude drops from around 5000 m to 100 m in less than 200 km. The tracking ability of Jason2 is better than RA2 at this mountain region. It is interesting to note that the ascending tracks (from RA2 is easier to recover from low elevation to high elevation than that of the reverse.

The plateau's glaciers and other geographical and ecological features serve as headwaters of several large rivers. The Ganges,

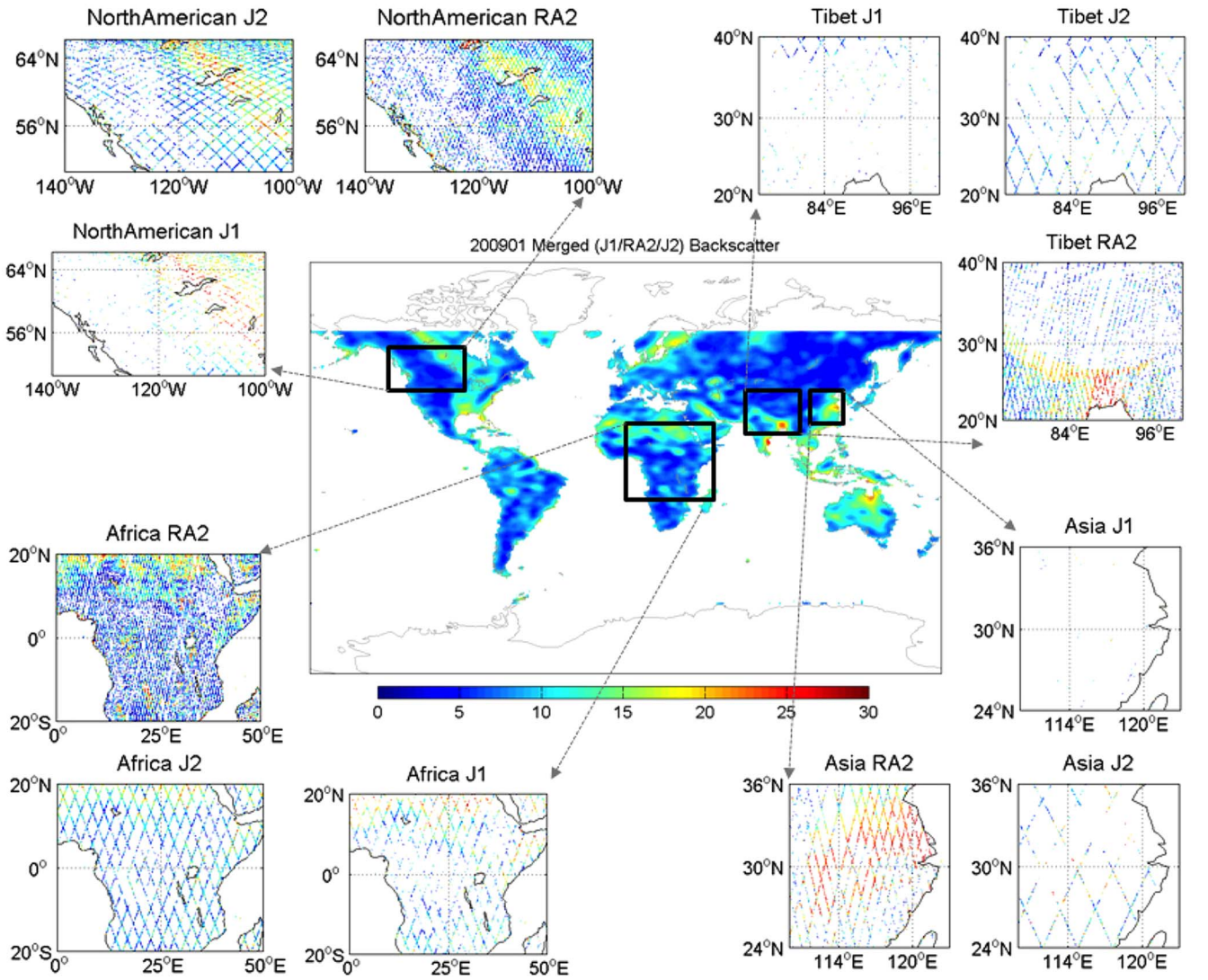

Fig. 7. Ku-band backscatter coefficient map (dB) of January 2009 of global merged data (a) and Tibet (b), (c), and (d); Asia (e), (f), and (g); Africa (h), (i), and (j); and North America (k), (l), and (m) for Jason1, Jason2, and Envisat RA2, respectively.

Brahmaputra, and their tributaries flow southeastward into the Bay of Bengal, which influence the vegetation and soil property around the rivers. The altimetry backscatter exhibits clearly seasonal changes. The mean value of the merged backscatter is 10.62 dB in July and 8.97 dB in January. Furthermore, the distribution of the high value is wider in July than in January.

African continent: From the north to south over the African continent, the land cover types exhibit a clear pattern that reflects the transition of the increasing vegetation from dessert/barren- shrubs- savannas- woody savannas to the evergreen broadleaf forest. The desert and barren regions in the north have higher backscatter value than vegetation, which is evident in the three altimeters measurement. As expected, the seasonal change from July to January is more obvious in the barren and shrub regions than in the evergreen broadleaf forest of the center and south part of the African continent. It is interesting to note that there is one low value region around 15° N, 12.5° E in the transition area from barren to savannas. We found that this region coincided with the location of Lake Chad, which is once one of the world's largest lakes. Its area has been reduced to less than 1540 km^2 nowadays. Although the area of the lake surface is not large, the surrounding area of the Lake Chad is an important agriculture area. The low value region shows the ecological characteristics of vegetation and soil around the lake.

North American continent: From the western mountains to the eastern Great Lakes and St. Lawrence lowlands over the North American continent, the merged backscatter shows not only that the spatial distributions from low to high but also the strong spatial consistency. The magnitude and coverage in the eastern lowlands are larger in July than in January. The mean value of the merged backscatter in this region is 10.62 dB in July and 8.97 dB in January The effect of ice or snow (enlarge the backscatter) does not appear because the measurements over ice or snow are excluded.

In the homogeneous areas at the kilometer scale, such as the desert and forest in Africa, the patterns of the Jason1, Jason2, and RA2 measurements are similar and agree with the merged result. For spatial heterogeneity areas, RA2 has better spatial sampling abilities for its dense ground track. In the Tibetan

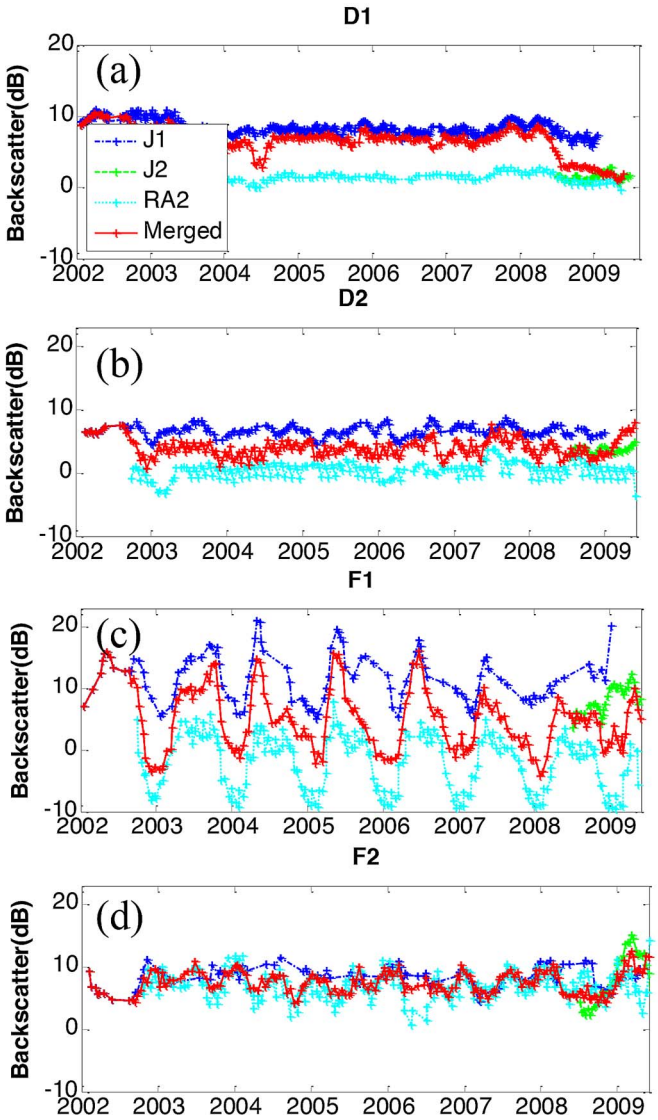

Fig. 8. Temporal backscatter profiles for the Ku-band obtained from (blue) Jason1, (green) Jason2, (cyan) Envisat RA2, and (red) merged results for the (a) Taklimakan Desert, (b) Badain Jaran Desert, (c) Lesser Khingan Forest, and (d) QiongZhong Forest from January 2002 to June 2009.

plateau, with its complex terrain, the tracking ability of Jason2 is superior. Therefore, the merged altimetry backscatter results have better spatial sampling due to the combination of the ground tracks of three altimeters.

2) Temporal signatures of backscatter results for selected desert and forest sites: To further examine the merged altimetry backscatter, two sites over desert and two sites over forest were selected because they are typical land covers with different seasonal variations. We did not analyze the global deserts or forests considering the limited tracking ability of the radar altimeter over complex terrain. The locations of the four sites are shown in Fig. 8(a). The Taklimakan Desert (D1: 39.40°N, 86.60° E) located in southwest China covers an area of 270 000 square km (approximately 1000 km long and 400 km wide) in the Tarim Basin. The annual precipitation ranges from 10 to 38 mm. The Badain Jaran Desert (D2: 40.30°N, 101.40° E) covers an area of 49 000 square km and is home to the tallest stationary dunes on earth. Between the tall dunes, there are as many as 114 inland lakes, with 74 perennial water lakes. The annual precipitation ranges from 50 to 60 mm. The two forest sites included the Lesser Khingan Forest and QiongZhong Forest, which correspond to types of boreal and subtropical forest, respectively. The Lesser Khingan Forest (F1: 48.58° N, 128.51° E) covers a mountain range located in the Heilongjiang Province of China and the adjacent parts of Russia. The forest is approximately 100 km wide and 400 km long, with an area of approximately 39 400 square km. The Lesser Khingan Forest is a mixed forest with primarily Larixgmelinii, Birch, and Korean pine as tree types. The QiongZhong Forest (F2: 19.10° N, 109.78° E) is located near the equator and is a typical natural evergreen forest.

Temporal backscatter profiles were extracted to analyze the radar response to variability in the selected surfaces over eight years. Fig. 8 shows the backscatter results for the Ku-band over the four sites from Jason1, Jason2, Envisat RA2, and the merged result. The merged backscatter curves lie between that of Jason1 and RA2 and follow a similar trend. The backscatter values for the Taklimakan Desert [see Fig. 8(a)] exhibit little variability over time, which is in agreement with a previous study [13]. The variability of these backscatter measurements was found to be the lowest among the four sites. The standard deviations for Jason1 and RA2 were 1.40 and 1.09 dB, respectively. However, the RA2 backscatter was less than zero, and the mean difference between Jason1 and RA2 was 6.76 dB. For the Badain Jaran Desert [see Fig. 8(b)], the backscatter variations were also low but larger than those of the Taklimakan Desert, which could result from the seasonal change in water supply, particularly from the lakes within the desert. For the Lesser Khingan Forest [see Fig. 8(c)], the mean values for Jason1, Jason2, RA2, and the merged backscatter were 11.61, 8.31, −2.05, and 5.19 dB, respectively. A strong seasonal variation in backscattering over the Lesser Khingan was observed. The standard deviations of the backscatter results for Jason1, Jason2, RA2 and the merged results were 3.92, 2.39, 4.47, and 6.90 dB, which strongly correlate with the seasonal evolution of the vegetation associated with the climate. The backscatter values reached a maximum in summer and a minimum in winter. For the QiongZhong Forest [see Fig. 8(d)], the backscatter results exhibited a more stable signal than observed for the Lesser Khingan Forest. The standard deviations of the Jason1, Jason2, RA2, and merged backscatter results were 1.69, 4.17, 2.19, and 3.93 dB, respectively. The mean values for the Jason1 (6.90 dB) and Envisat RA2 backscatter results (7.96 dB) were similar.

B. Altimetry Backscatter Measurements Compared With LAI and SCAT $\sigma 0$

To relate the altimetry backscatter values to geophysical parameters, the temporal variations of the merged altimetry backscatter data with respect to the LAI obtained from an optical sensor (SPOT/VEGETATION) and the backscatter observed at an oblique angle by a scatterometer (QuikSCAT) were examined for seven selected sites with various vegetation types.

LAI is defined as half the total foliage area per unit ground surface area [30]. It is a dimensionless ratio (m2/m2) describing

TABLE I
MEAN VALUES OF LAI, CORRELATION COEFFICIENTS, AND RANGES OF MERGED ALTIMETER BACKSCATTER (ALT) AND QUIKSCAT HH POLARIZATION BACKSCATTER (SCATH) RESULT FROM 2002 TO 2007 AT SEVEN SELECTED SITES

Site	Latitude (degree)	Longitude (degree)	Surface Type	mean LAI	Correlation Coefficient			Range	
					ScatH -LAI	Alt -LAI	Alt -ScatH	Alt (dB)	ScatH (dB)
b	12.629	10.977	Grasslands	0.22	0.87	0.65	0.71	6.18	6.78
c	-25.332	148.100	Woody savannas	0.59	0.67	0.19	0.24	12.67	2.37
d	10.528	-3.976	Savannas	0.91	0.94	0.64	0.69	12.99	2.57
e	58.191	77.636	Mixed forest	1.47	-0.14	0.44	-0.63*	19.13	1.24
f	59.742	58.633	ENF	1.57	-0.27	0.01	-0.58*	17.78	3.87
g	-24.282	-62.584	DBF	1.64	0.48	0.56	0.50	13.87	4.78
h	1.776	12.677	EBF	2.84	-0.10	-0.01	-0.11	5.47	1.30

the leaf area covering a unit of ground area and indicates the number of layers of full covered leafy vegetation between the ground and the top of the canopy that are available to absorb and convert solar energy. The CYCLOPES LAI product [31] produces global spatial data, with a 1-km resolution, that cover the period of 1999–2007 with a time step of ten days; these data are derived from measurements acquired by the SPOT/VEGETATION sensor. The SeaWinds/QuikSCAT σ^0.

Browse Product [32] provides a Ku-band normalized backscatter coefficient at an incidence angle of 46° (HH) and 54.1° (VV) with 22.5-km resolution over a one-day period. Because the lowest time resolution is ten days for the LAI and the lowest spatial resolution is 0.5° for the merged altimetry backscatter results, the three data sets (LAI, merged altimetry σ^0 and QuikSCAT σ^0) were interpolated to every ten days and 0.5° from January 2002 to December 2007.

Throughout the time-series analysis, the altimeter and scatterometer backscatter measurements were used as a direct representation of the canopy forest structure and water content of different layers to avoid an indirect estimation and validation of water content or structure. The name of the selected sites, the surface types and the main statistics (mean, range-difference between the maximum to minimum value, and correlation coefficient) of the different temporal series are listed in Table I. The general location of the sites is shown on the map [see Fig. 9(a)] with a star and the associated letter referenced to the next figures. Results of the temporal profiles obtained for the merged altimeter backscatter data, scatterometer backscatter data, and the LAI are shown in Fig. 9.

The mean value of LAI in increasing order corresponded to grasslands, woody savannas, savannas, mixed forest, ENF, DBF, and EBF, which indicates the leafy part of vegetation of these sites are more and more dense. The QuikSCAT backscatter value is strongly correlated to LAI, with correlation coefficient of 0.87, 0.64, 0.94 at the grassland, woody savannas, savannas, which is agreed to previous observations [33, 34].

A clear correlation between merged altimetry backscatter and LAI as QuikSCAT backscatter value is also found for seasonal vegetation of grassland, Savannas, mixed forest, and DBF, with the correlation coefficients of 0.65, 0.64, 0.44, and 0.56. It is interesting to note that the fluctuations in the curves of altimetry backscatter and LAI are not completely synchronized. The altimetry backscatter declined by about 4–5 dB at QuikSCAT σ^0 and LAI peaks in Fig. 9(d), (e), and (g). These decreases could be caused by a reduction in the moisture of the low-layer vegetation or soil during the growing season.

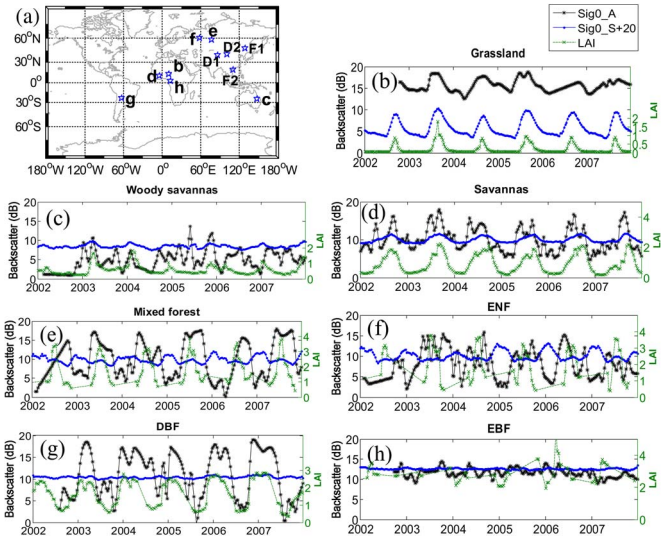

Fig. 9. The locations of the selected sites (a). The temporal evolution of the merged altimetry backscatter (left axis, black line with asterisk) compared with that of the QuikSCAT HH polarization backscatter plus 20 dB (left axis, blue line with dot) and with the LAI (right axis, green line with cross) for grassland (b), woody savannas (c), savannas (d), mixed forest (e), evergreen needleleaf forest (ENF) (f), deciduous broadleaf forest (DBF) (g), and evergreen broadleaf forest (EBF) (h) from 2002 to 2007.

As expected, the correlations are low for the EBF (g) because the EBF near the equator is stable, without significant seasonal fluctuations. It is noted that for the mixed forest and ENF, the correlations between merged altimetry backscatter and QuikSCAT backscatter are -0.63 and -0.58, respectively. Unlike merged altimetry backscatter and LAI, the QuikSCAT backscatter is not edited out the snow or ice covered data. Fig. 9(e) and (f) show that the QuikSCAT backscatter results at location (e) and (f) is high in winter and low in summer, in contrast to the other five locations. This is due to the appearance of ice or snow because locations (e) and (f) are at latitudes near 60 N.

The range value indicates the dynamic response extent of the backscatter data. It can be seen that the range values of altimetry backscatter is overall larger than the scatterometer backscatter. For the seasonal vegetation, the largest range of QuikSCAT is at the Grassland of 6.78 dB, which is understandable since the backscatter observation in Ku-band at 40°is easily saturated. However, for the altimeter backscatter, the largest range value is at mixed forest of 19.13 dB, followed by ENF (17.78 dB), DBF (13.87 dB), savannas (12.99 dB), woody savannas (12.67 dB),

grassland (6.18 dB), and EBF (5.47 dB). This indicates that the altimetry backscatter is more sensitive to the vegetation seasonal evolution, which is not necessary caused by the change of leaves, but also by the changes of vegetation fractional cover, structure, sizes, and water content or wet biomass. All those geophysical parameters may be represented by the aerodynamic roughness. The potential of altimetry backscatter to obtain quantitative results on aerodynamic roughness length will be further discussed in another paper.

Therefore, the scatterometer backscatter was more highly correlated with the LAI than the altimeter backscatter due to the different contributions from vegetation and soil at different observation geometries. The backscatter observed from an oblique observation (scatterometer) is primarily determined by the dielectric properties of the leaves of the canopy surface layer, whereas the nadir view (altimeter) is sensitive to roughness changes in the deeper layers.

V. Conclusion and Perspectives

The potential of multialtimeter backscatter measurements for land surface studies has been investigated. To improve the poor spatial and temporal resolution of a single altimeter, backscatter measurements of Jason1, Jason2, and Envisat RA2 were used to generate a first $0.5^\circ \times 0.5^\circ$ multiradar altimeter backscatter map covering 66°N to 66°S with an interval of six days from January 2001 to June 2009. The analysis of four RA2 retracker backscatter results indicates that four RA2 σ^0 values show large variability. The backscatters of the Ice1 and SeaIce retrackers were larger than those of the Ocean and SeaIce and also showed a significant degree of correlation with each other. The backscatter from the Ocean retracker was used in merging with the Jason1 and Jason2 data.

To evaluate the merged altimetry backscatter, we analyzed the results of three single altimeter and the merged results at regional patterns and their seasonal variations. The merged altimetry backscatter results have better spatial sampling than that of the single one, particularly for spatial heterogeneity areas with complex terrain. The merged altimetry backscatter exhibits a stable signal over deserts and rain forest.

We further compared the merged altimetry backscatter with LAI and scatterometer backscatter to relate the altimetry backscatter to geophysical parameters with the help of soil and vegetation model simulations. It was shown that the temporal variations are consistent with those of LAI derived by the optical sensor and scatterometer backscatter for seasonal vegetation. However, their range of values and responses to seasonal change can be significantly different. The merged altimetry backscatter has a larger dynamic range than scatterometer backscatter, which is not only associated with the leafy part of vegetation, but also with land cover type, vegetation fractional cover, structure, sizes, and water content or wet biomass.

Despite its low spatial resolution (km), the usefulness of the Ku-band in altimetry for monitoring vegetation dynamics is shown. We have only evaluated the merged backscatter in a qualitative way by using a simple vegetation model and by comparing them with LAI. Further studies utilizing sophisticated model specified for radar altimetry over vegetation and field geophysical parameter measurements are needed for the quantitative descriptions on how to derive the important geophysical parameters, such as aerodynamic roughness.

Acknowledgment

The authors would like to thank the AVISO for providing the Jason1/2 altimeter data and ESA for the Envisat RA2 altimeter data. The authors also thank the anonymous reviewers for their constructive comments, which helped to significantly improve this paper.

References

[1] B. D. Chelton, J. C. Ries, B. J. Haines, L. L. Fu, and A. Cazenave, "Satellite altimetry," in *Satellite Altimetry and Earth Sciences*. San Diego, CA, USA: Academic, 2001, pp. 1–131.

[2] B. Legresy and F. Remy, "Surface characteristics of the Antarctic ice sheet and altimetric observations," *J. Glac.*, vol. 43, pp. 197–206, 1997.

[3] D. Alsdorf, C. M. Birkett, T. Dunne, J. Melack, and L. Hess, "Water level changes in a large Amazon lake measured with spaceborne radar interferometry and altimetry," *Geophys. Res. Lett.*, vol. 28, no. 14, pp. 2671–2674, Jul. 2001.

[4] F. Frappart, S. Calmant, M. Cauhope, F. Seyler, and A. Cazenave, "Preliminary results of ENVISAT RA-2 derived water levels validation over the Amazon basin," *Remote Sens. Environ.*, vol. 100, no. 2, pp. 252–264, Jan. 2006.

[5] P. A. M. Berry, J. D. Garlick, and R. G. Smith, "Near-global validation of the SRTM DEM using satellite radar altimetry," *Remote Sensing of Environment*, vol. 106, no. 1, pp. 17–27, Jan. 2007.

[6] P. A. M. Berry, "Topography from land radar altimeter data: Possibilities and restrictions," *Phys. Chem. Earth(A)*, vol. 25, no. 1, pp. 81–88, 2000.

[7] P. L. Frison and E. Mougin, "Use of ERS-1 wind scatterometer data over land surfaces," *IEEE Trans. Geosci. Remote Sens.*, vol. 34, no. 2, pp. 550–560, Mar. 1996.

[8] C. Oliver, *Spaceborne Radar Remote Sensing: Applications and Techniques*. New York, NY, USA: IEEE Press, 1988.

[9] S. Sassan *et al.*, "Persistent effects of a severe drought on Amazonian forest canopy," *Proc. Nat. Acad. Sci.*, vol. 110, no. 2, pp. 565–570, 2012.

[10] J. Ridley, F. Strawbridge, R. Card, and H. Phillips, "Radar backscatter characteristics of a desert surface," *Remote Sens. Environ.*, vol. 57, no. 2, pp. 63–78, Aug. 1996.

[11] S. M. S. Bramer, C. P. D. Johnson, and P. A. M. Berry, "Analysis of ENVISAT RA-2 Backscatter over Natural Land Calibration Targets," presented at the Envisat ERS Symp., Noordwijk, The Netherlands, 2004.

[12] S. M. S. Bramer, P. A. M. Berry, J. A. Freeman, and B. Rommen, "Global Analysis of Envisat Ku and S Band Sigma0 over all Surfaces," presented at the Envisat Symp., Montreux, Switzerland, 2007.

[13] F. Papa, B. Legresy, and F. Remy, "Use of the Topex-Poseidon dual-frequency radar altimeter over land surfaces," *Remote Sens. Environ.*, vol. 87, no. 2/3, pp. 136–147, Oct. 2003.

[14] N. Picot, K. Case, S. Desai, and P. Vincent, *AVISO and PODAAC User Handbook IGDR and GDR Jason Products*. Washington, DC, USA: NASA, 2003, p. 8.

[15] J. P. Dumont *et al.*, *OSTM/Jason-2 Products Handbook*. Washington, DC, USA: NASA, 2009.

[16] ESA, ENVISAT RA2/MWR Product Handbook V2.2 2007.

[17] M. A. Friedl *et al.*, "Global land cover mapping from MODIS: algorithms and early results," *Remote Sens. Environ.*, vol. 83, pp. 287–302, 2002.

[18] F. Ulaby, R. Moore, and A. Fung, *Microwave Remote Sensing—Active and Passive Vol III.*. Norwood, MA, USA: Artech House, 1986.

[19] L. D. Witter and B. D. Chelton, "A Geosat altimeter wind speed algorithm and a method for altimeter wind speed algorithm development," *J. Geophys. Res.*, vol. 96, no. C5, pp. 8853–8860, May 1991.

[20] D. Shepard, "A two-dimensional interpolation function for irregularly-spaced data," in *Proc. ACM Nat. Conf.*, 1968, pp. 517–524.

[21] K. S. Chen *et al.*, "Emission of rough surfaces calculated by the integral equation method with comparison to three-dimensional moment method simulations," *IEEE Trans. Geosci. Remote Sens.*, vol. 41, no. 1, pp. 90–101, Jan. 2003.

[22] A. K. Fung, *Microwave Scattering and Emission Models and their Applications*. Norwood, MA, USA: Artech House, 1994.

[23] W. Tzong-Dar and C. Kun-Shan, "A reappraisal of the validity of the IEM model for backscattering from rough surfaces," *IEEE Trans. Geosci. Remote Sens.*, vol. 42, no. 4, pp. 743–753, Apr. 2004.
[24] J. C. Shi *et al.*, "A parameterized multifrequency-polarization surface emission model," *IEEE Trans. Geosci. Remote Sens.*, vol. 43, no. 12, pp. 2831–2841, Dec. 2005.
[25] E. P. W. Attema and F. T. Ulaby, "Vegetation modeled as a water cloud," *Radio Sci.*, vol. 13, no. 2, pp. 357–364, Mar./Apr. 1978.
[26] K. C. McDonald, M. C. Dobson, and F. T. Ulaby, "Using Mimics to model L-band multiangle and multitemporal backscatter from a walnut orchard," *IEEE Trans. Geosci. Remote Sens.*, vol. 28, no. 4, pp. 477–491, Jun. 1990.
[27] G. Q. Sun and K. J. Ranson, "A three-dimensional radar backscatter model of forest canopies," *IEEE Trans. Geosci. Remote Sens.*, vol. 33, no. 2, pp. 372–382, Mar. 1995.
[28] K. C. Mcdonald and F. T. Ulaby, "Radiative transfer modelling of discontinuous tree canopies at microwave frequencies," *Int. J. Remote Sens.*, vol. 14, no. 11, pp. 2097–2128, 1993.
[29] J. M. CHEN and T. A. BLACK, "Defining leaf area index for non-flat leaves," *Plant, Cell Environ.*, vol. 15, no. 4, pp. 421–429, May 1992.
[30] F. Baret *et al.*, "LAI, fAPAR and fCover CYCLOPES global products derived from VEGETATION: Part 1: Principles of the algorithm," *Remote Sens. Environ.*, vol. 110, no. 3, pp. 275–286, Oct. 2007.
[31] D. G. Long, "Reconstruction and Resolution Enhancement Techniques for Microwave Sensors," in *Frontiers Remote Sensing Information Processing*, C. H. Chen, Ed. Singapore: World Scientific, 2003.
[32] S. Frolking, M. Fahnestock, T. Milliman, K. McDonald, and J. Kimball, "Interannual variability in North American grassland biomass/productivity detected by SeaWinds scatterometer backscatter," *Geophys. Res. Lett.*, vol. 32, no. 21, pp. 1–5, 2005.
[33] G. Macelloni, S. Paloscia, P. Pampaloni, and E. Santi, "Global scale monitoring of soil and vegetation using SSM/I and ERS wind scatterometer," *Int. J. Remote Sens.*, vol. 24, no. 12, pp. 2409–2425, 2003.

Le Yang was born in Sichuan, in China, 1981. She received the B.S. degree in applied physics and the Ph.D. degree in computer science from the Nanjing University of Science and Technology, Nanjing, China, in 2004 and 2009, respectively. From 2006 to 2009, she pursued the Ph.D. degree from the Second Oceanographic Institute, State Oceanographic Administration, Hangzhou, China.

Since 2009, she has been an Assistant Researcher with the Institute of Remote Sensing and Digital Earth, Chinese Academy of Sciences, Beijing, China. Her research interests include radar altimetry and its associated retrieve processing, and vegetation modeling and parameter retrieval by synergy optical and microwave remote sensing data.

Qinhuo Liu (M'97) received the B.Sc. degree in hydrogeology and engineering geology from Southwest Jiaotong University, Chengdu, China, in 1988, and the M.Sc. degree in cartography and remote sensing and Ph.D. degree in atmospheric physics from Peking University, Beijing, China, in 1994 and 1997, respectively.

He was with National Institute for Agricultural Research INRA of France in 1998; Boston University, Boston, MA, USA, in 1999; the University of Maryland, College Park, MD, USA, in 2004; and George Mason University, Fairfax, VA, USA, in 2010 as a Visiting Scholar. Since 1997, he has been with the Institute of Remote Sensing Applications, Chinese Academy of Sciences, Beijing. He is currently a Professor and Deputy Director with the State Key Laboratory of Remote Sensing Science, Institute of Remote Sensing and Digital Earth, Chinese Academy of Sciences. His research interests include radiation transfer modeling, quantitative remote sensing inversion, assimilation, and applications.

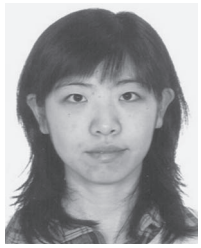

Jing Zhao received the B.S. degree in geography information system and the M.S. degree in cartography and geography information system from Jilin University, Changchun, China, in 2007 and 2009, respectively, and the Ph.D. degree in cartography and geography information system from the Institute of Remote Sensing and Digital Earth, Chinese Academy of Sciences, Beijing, China, in 2013.

She is currently a Research Assistant with the Institute of Remote Sensing and Digital Earth, Chinese Academy of Sciences, Beijing. Her primary research interests include canopy saturation analysis and leaf area index inversion from remote sensing.

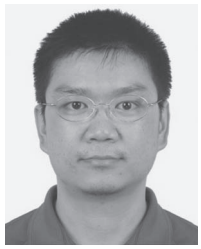

Lifeng Bao received the B.S. degree in geodesy from the Wuhan Technical University of Surveying and Mapping, Wuhan, China, in 2000 and the Ph.D. degree in geodesy from the Institute of Geodesy and Geophysics, Chinese Academy of Sciences, Wuhan, in 2005.

From 2006 to 2012, he has been with the Institute of Geodesy and Geophysics, Chinese Academy of Sciences, as an Associate Professor. Since 2012, he has been a Professor with the State Key Laboratory of Geodesy and Earth's Dynamics, Institute of Geodesy and Geophysics, Chinese Academy of Sciences.